Hindawi
Advances in Meteorology
Volume 2020, Article ID 8395269, 16 pages
https://doi.org/10.1155/2020/8395269

Research Article

Synergy Effects of the Indian Summer Monsoon and the Tibetan Plateau Heating on Summer Rainfall over North China

Siwen Zhao,[1] **Jie Zhang**,[1] **and Zhihong Lv**[2]

[1]*Key Laboratory of Meteorological Disaster, Ministry of Education (KLME), Joint International Research Laboratory of Climate and Environment Change (ILCEC), Collaborative Innovation Center on Forecast and Evaluation of Meteorological Disasters (CIC-FEMD), Nanjing University of Information Science & Technology, Nanjing 210044, China*
[2]*Fushun Meteorological Bureau, Fushun 113000, China*

Correspondence should be addressed to Jie Zhang; gs-zhangjie@163.com

Received 11 September 2019; Accepted 4 February 2020; Published 19 March 2020

Academic Editor: Ismail Gultepe

An analysis based on July-August precipitation reveals that there is a tripole pattern of the precipitation distribution, that is, significantly increased rainfall over North China (NC) is related to the increased rainfall over the Indian subcontinent (IS) and the decreased rainfall over the southeastern Tibetan Plateau (TP) and vice versa, that corresponds to the Indian summer monsoon (ISM) and TP heating pattern, which are interactive. Therefore, it is necessary to investigate the effect of NC rainfall-related atmospheric circulation and the physical linkage with the two thermal forcings together. The linear baroclinic model (LBM) is applied to determine the dynamics of the process. The results show that an enhanced ISM is accompanied by reduced TP heating, favors convection and easterly anomaly over the IS, and produces a Gill-type Rossby wave that affects the vorticity over North Africa. Meanwhile, there is another Rossby wave originating in North Africa and moving eastward to the Pacific Ocean, which interferes with circulation at mid- to high-latitudes, i.e., it strengthens the cyclone over the Baikal region and stretches the western Pacific subtropical high (WPSH) northward to northeastern Asia, and results in abundant water vapor transported to NC. Furthermore, the strong convection over the IS excites the Kelvin waves over the equatorial region, which moves eastward and generates anticyclones over Philippines, consequently leading to the Pacific-Japan (PJ) pattern. The PJ pattern cooperates with the wave train at midlatitudes, resulting in abundant water vapor being transported to NC. The summer rainfall over NC is therefore modulated by synergistic effect of both the ISM and TP heating.

1. Introduction

North China (NC) is located at mid-to high-latitudes between the Baikal region and the northwestern Pacific Ocean; the climate variability here in summer is very large and is affected by atmospheric circulation anomalies such as blockings at high-latitudes over both the tropical and extratropical regions [1], westerly wave trains [2], western Pacific subtropical high (WPSH) [3], and Asian summer monsoons [4–6]. NC is a densely populated, resource-rich, and economically developed region in China and has a great demand for water [7]. Summer precipitation contributes more than 70% of the annual total precipitation in NC [8] and exhibits substantial interannual to decadal variations, resulting in more sensitivity to water shortages. Therefore, it is essential to predict the precipitation over NC.

The precipitation variability in NC is closely related to stationary external Rossby waves [9, 10] that are excited by divergence caused by orthography and thermal forcing [11] and quickly disperse along the westerly jet stream [12], further affecting the global atmospheric circulation anomalies. However, the effect factors at mid-to high-latitudes are complex and diverse, and the wave trains in extratropical regions are considered to be responses to the tropical heating anomalies [13, 14]. Many studies thus focused on the heating sources in the tropics such as the Indian summer monsoon

(ISM) and suggested that increased precipitation over the Indian subcontinent (IS) played an important role in the boreal atmosphere during summer.

Many previous publications have focused on the relationship between precipitation over NC and the ISM. Kripalani and Singh [15] noted that the rainfall over NC is highly related to rainfall over India and suggested to take the subtropical ridge over the Indian region as an important predictor over India as well as over NC. Wang et al. [16] and Ding and Wang [9] commented that the rainfall shows synchronous anomalies over the IS and NC during summer. Liu and Ding [17] also utilized the model to simulate the precipitation teleconnection between India and North China. Various studies documented that the ISM affected the summer climate in East Asia through a midlatitude wave train along the East Asian upper tropospheric westerly jet stream, causing differences in atmospheric circulation and water vapor transport [18, 19]. The results further revealed that an enhanced ISM could generate anomalous cyclonic circulation over the Mediterranean Sea in the upper layer [20, 21] and stimulated a continuous downstream air flow, i.e., a silk road pattern [22], with a barotropic anticyclonic anomaly over East Asia, leading to more water vapor being transported northward along the western periphery of the WPSH [23]. However, the position and intensity of the ISM, which lead to precipitation over NC, exhibit large variabilities in addition to land-sea thermal contrasts and are affected by atmospheric internal dynamic processes [24] and El Niño-Southern Oscillations (ENSO) [25]. The thermal forcing of the Tibetan Plateau (TP) also plays a decisive role through air pumping [26–28]. Moreover, the TP also has a considerable influence on the boreal circulation and precipitation as a significant surface and atmospheric heating source in summer [29, 30], which, therefore, is also considered.

The change in TP diabatic heating, especially latent heating released by rainfall in summer, has a profound influence on the seasonal circulation and the interannual changes of the Northern Hemisphere [31], and it has considerable influence on the precipitation over NC during the summer time. Observational studies have shown that increased TP heating can intensify East Asian summer monsoons, which contribute to the upward trend of monsoon rainfall over NC [32, 33]. Heating on the TP will trigger two waves. One wave travels downstream along the westerly jet stream and the other wave spreads along the low-level southwesterly monsoon flow to the South China Sea [34]. The west one results in an anticyclone over NC, leading to less precipitation there [35].

Despite the effect of TP thermal forcing on the ISM, the ISM can also affect summer rainfall over the TP over a wide range of time scales [36, 37], which is modulated by atmospheric processes over the midlatitudes [38] and incoming water vapor transport [39, 40], further affecting the thermal condition of the TP.

Prior to the current study of precipitation over NC, most studies have typically involved only one single influence factor because it is difficult to identify the main influencing factors, which vary but may not be considered. Because of the interactive relationship between the TP thermal forcing and the ISM, it is reasonable to regard both as one phenomenon or to assume that they are one system. Additionally, the investigations on the role of tropical heating have been limited to only revealing the correlation; thus, the mechanism is unclear.

Based on the above discussions, the objectives of this study were to determine the precipitation distribution pattern during summer, investigate the effect of the ISM and TP heating on the precipitation over NC, and utilize a model to understand the mechanism. This paper focuses on the variability of the midlatitude wave train, which will help to interpret extratropical responses to the tropical heating anomalies in Asia. A more practical motivation for this study is that the precipitation over NC can be fully and accurately predicted.

The structure of this paper is as follows: Section 2 describes the data and methods. Section 3 shows the tripole pattern distribution and the related circulation. In Section 4, we describe the model experiments performed to obtain the circulation response to different forcing. Section 5 presents the wave activity flux to analyze the propagation of the wave. Brief conclusions and discussions are provided in Section 6.

2. Materials and Methods

In this study, we focused on the concentration period (July-August, JA) of summer rainfall when the precipitation mode is most typical, and a wave-like pattern is also often observed over Eurasia.

The following datasets were used in this study. (1) The daily precipitation data (APHRO) were derived from the Asian Precipitation -Highly-Resolved Observational Data Integration towards Evaluation of the Water Resources (APHRODITE). The subset of APHRO covered Monsoon Area (60°N-150°N/15°S-55°N), APHRO_MA_V1101, was used. The product includes daily rainfall from 1951 to 2007, with a spatial resolution of $0.25^\circ \times 0.25^\circ$. The APHRO rainfall shows fair applicability in the TP and surrounding areas because of its high resolution and improvement in interpolation [41]. To verify the results, the global rainfall dataset, the Global Precipitation Climatology Centre monthly (GPCC) mean rainfall data, was derived from the National Oceanic and Atmosphere Administration (NOAA) at a resolution of $1.0^\circ \times 1.0^\circ$, and the data were chosen for the period of 1901–2013 (http://www.esrl.noaa.gov/psd/; [42]). Monthly mean rainfall from the Global Rainfall Climatology Project (GPCP) analysis dataset version 2.3 from 1979 to 2017 (http://gpcp.umd.edu./; [43]) was used. (2) The European Centre for Medium-Range Weather Forecasts (ECMWF) Interim Re-Analysis monthly atmospheric reanalysis data included geopotential height and zonal and meridional winds at 200 hPa, 500 hPa, and 850 hPa on a $1.5^\circ \times 1.5^\circ$ grid for 1979–2017, which were obtained from the ECMWF (http://apps.ecmwf.int/datasets/; [44]).

The main statistical tools used in this study included empirical orthogonal function (EOF) analysis, correlation analysis, and regression analysis. Linear trends were removed from all the data before the regression and

correlation analyses were performed. The North test was used to examine the stability of each EOF [45]. Student's t test was performed to calculate the significance in the correlation and regression analyses.

In this paper, the inverse algorithm was used to calculate the apparent heat source (Q_1) and apparent moisture sink (Q_2) of the atmosphere from 1979 to 2017, which could be obtained from the following formula [46]:

$$Q_1 = C_p\left[\frac{\partial T}{\partial t} + \vec{V} * \nabla T + \left(\frac{p}{p_0}\right)^{\kappa}\omega\frac{\partial\theta}{\partial p}\right],$$
$$Q_2 = -\frac{L}{C_p}\left[\frac{\partial q}{\partial t} + V\cdot\nabla q + \omega\frac{\partial q}{\partial p}\right], \quad (1)$$

where $\kappa = R/C_p$, R is the dry air Gas constant, C_p is the specific heat at constant pressure, θ is the potential temperature, t is the temperature, q is the mixing ratio of water vapor, v is the horizontal wind, and L is the latent heat of condensation. Term Q_1 represents the heating rate of air per unit mass in unit time, and term Q_2 represents the heating rate caused by the heat released by condensation of water vapor per unit mass in unit time. In this paper, the integration height from the ground (surface pressure, P_S) to the top (100 hPa) of the convection layer was chosen. Q_1 was used to represent the integrated atmospheric apparent heat source, and Q_2 was used to represent the integrated apparent moisture sink. When water vapor decreased due to condensation, the latent heat is released and Q_2 was positive; otherwise, it was negative.

The numerical experiments performed in this study were based on the linear baroclinic model (LBM) that was described in detail in Watanabe and Kimoto [47, 48]. Many studies show that the LBM is a useful tool to diagnose how the atmosphere dynamically reacts to the prescribed forcing, which is in general agreement with observations [19, 49]. To clarify the role of dynamic processes, we utilized the dry LBM based on time integration of the linear model with realistic orography. The resolution used here was a triangular truncation of 42 waves (T42), and its horizontal resolution was approximately $2.8^\circ \times 2.8^\circ$ with 20 equally spaced sigma levels (L20). The basic background state of the experiment was the JA climate average field of the ERA-Interim data for 1979–2017. The boundary conditions and initial conditions were determined by the model. An important feature of the model was that the time integration was set at up to 30 days because the response approached a steady state near day 15 to 20. Here, we took the day 15 as steady results.

3. Observed Linkage among Rainfalls over the IS, TP, and NC

3.1. Rainfall Tripole Pattern in Summer time. To identify the rainfall distribution patterns, we applied EOF analysis to the covariance metric of JA precipitation. Figure 1(a) shows the leading rainfall variability pattern over Asia based on APHRO data. The leading mode (EOF1) accounts for 15.1% of the total variance and is well separated from the other modes evaluated by the North test. The pattern (shown as "+−+" in Figure 1(a)) is a tripole pattern that extends from the IS across the southeastern TP to NC. This tripole pattern is available when the EOF analysis is applied to the GPCC rainfall data from 1940 to 2013 (Figure not shown), and it is defined as an IS-NC pattern by Zhang et al. [50]. The principal component corresponding to the leading spatial pattern (PC1) is shown in Figure 1(b), which indicates the tripole pattern rainfall has discernable interannual variations superposed upon it. To facilitate our analysis, we define the IS rainfall index (ISR) as the normalized area average rainfall in the region of 75°E–85°E, 20°N–26°N in JA, with the North China rainfall index (NCR) for the domain of 107°E–120°E, 37°N–44°N and the rainfall index of the southeastern TP (TPR) is defined over the region of 85°E–95°E, 28°N–31°N. The simultaneous rainfall associated with the ISR features a significant distribution, as mentioned above. The tripole pattern is still significant when the GPCC data are applied to calculate the correlation of ISR with rainfall (Figure 1(c)). The negative correlation center of precipitation in TP is in the southeastern foot of the mountain, just the region we picked. In addition, we notice that there are also obvious positive correlation areas with ISR in Southeast Asia from Figures 1(a) and 1(c). It may be related to the water vapor channel under this pattern and will be discussed later. Figure 1(d) displays the time series for the ISR (the black solid line), the NCR (blue dashed line), and the TPR (the red dashed line). The out-of-phase relationship of rainfall between Indian monsoon and NC is a well-known teleconnection pattern, and the correlation coefficient between NCR and ISR is 0.30, while −0.16 is not significant with TPR. What role does the TP play? Then, we calculate the correlation coefficient between the ISR and the TPR, which is −0.6, and it supports the point that they are synergistic and affect the climate in NC.

The ISR exhibits a reverse variation with precipitation over the southeastern TP, implying a reverse latent heat distribution. The latent heat of condensation associated with the large amount of rainfall in both the IS and the TP plays a vital role in driving the atmosphere circulation in northern hemisphere [27]. Thus, to determine the underlying reason for the tripole pattern and its effect, we examine the associated atmospheric circulation anomalies in Section 3.2.

3.2. Associated Atmospheric Circulations. Figure 2 shows the regression patterns of the atmospheric circulation and rainfall onto PC1. When PC1 is positive, precipitation increases in the IS and NC, corresponding to weakened South Asian High (Figure 2(a)). There are strong anticyclonic anomalies near Central Asia, which indicates strong divergence. The basic distribution of summer circulation is shown in Figure 2(b) as contours. There are obvious trough and ridge activities in the westerly belt, and the WPSH is about 30°N in latitude. In the mid-troposphere (Figure 2(b)), the WPSH is significantly northwestward, there are obvious westerly anomalies in NC, with warm and wet air transported. Meanwhile, the negative anomaly near Lake Baikal deepens the trough and transports dry and cold air from

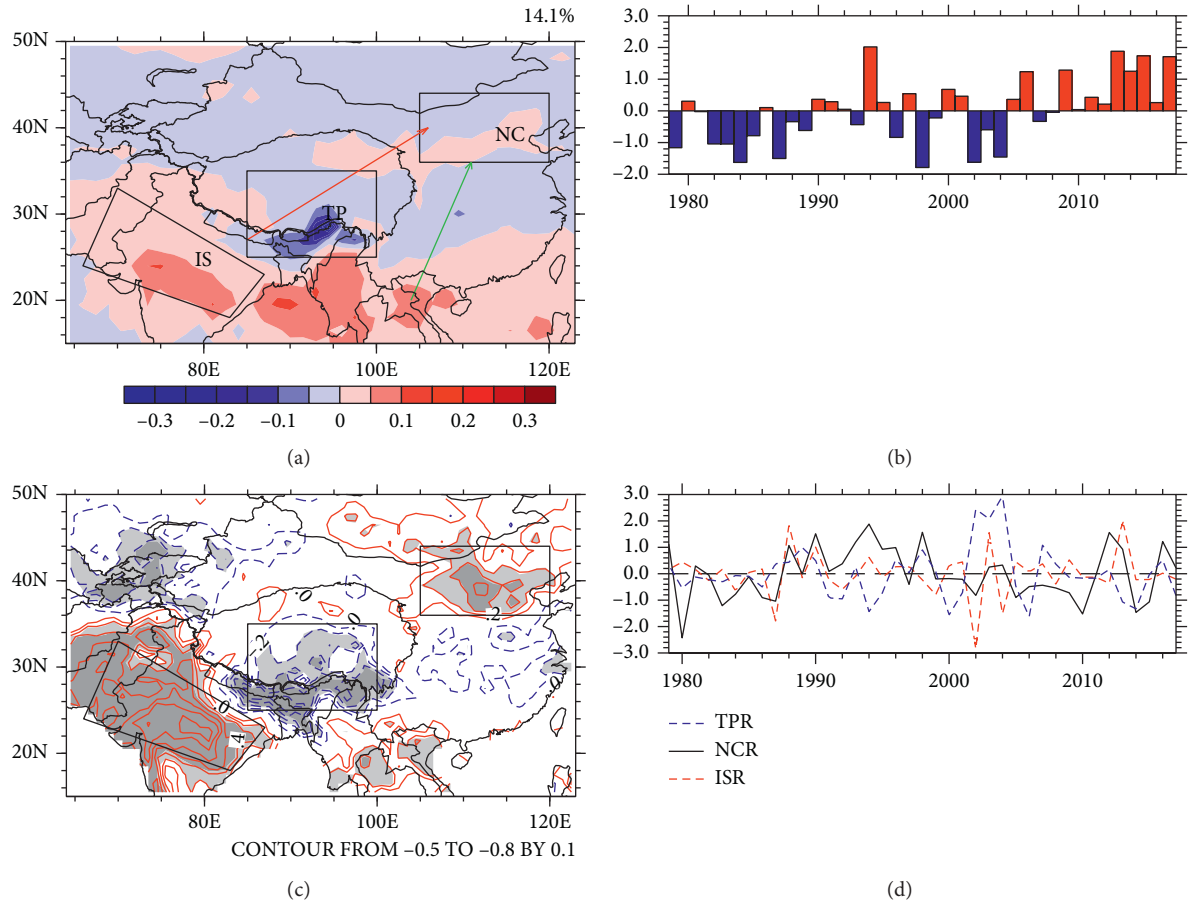

Figure 1: (a) Spatial pattern of the first EOF analysis applied to July-August (JA) APHRODITE rainfall from 1951 to 2007. (b) Principal component corresponding to spatial pattern in (a). (c) Geographical distribution map of the correlation coefficients between JA GPCC rainfall from 1940 to 2013 and the India Subcontinent Rainfall (ISR), dark (light) shadings indicate values exceeding 99% (90%) confidence levels through student's t test. (d) The time series of the ISR (red dashed line), rainfall over North China (NCR) (blue dashed line) and southeastern Tibetan Plateau Rainfall (TPR) (black solid line).

Siberia to NC. There are divergence anomalies over the TP and the wind speed is small, which is coherent with Jiang [37]. In northern India, the westward flow is obvious. There are significant cyclonic anomalies leading to the increase of convection. As for term of water vapor transport, it is basically consistent with the distribution of precipitation anomalies (Figure 2(c)). One branch of water vapor is transported from the cross-equatorial airflow to India, and another branch is transported to India around the northern topographic line of the TP from the Bay of Bengal, while there is less water vapor to the TP, corresponding to less precipitation. There is also significant water vapor transported to NC. To further illustrate circulation anomalies related to rainfall in these three regions, we compare the regressed atmospheric circulation anomalies against the NCR, TPR, and ISR, as shown in Figure 3.

Figure 3(a) shows the regression map of atmosphere circulation with regard to the simultaneous NCR, which is related to ascending precipitation over NC. There is a well-organized zonal wave train spanning from Central Asia to the Pacific Ocean with anomalous anticyclones in the Mediterranean, Central Asia, and Northeast Asia, separated by cyclonic anomalies. The anomalous cyclone strengthens the trough and conveys cold dry air into NC. Besides, the anomalous anticyclone over Northeast Asia is conducive to the WPSH northward and causes more moisture transported to NC, consequently leading to the northward shifting of the distribution of precipitation in East China. Moreover, the anomalous anticyclone diverged over the TP in the lower troposphere (Figure 4(a)), suggesting a decrease in precipitation because the southerly movement and convergence are significant for increased rainfall in the tropics since the air temperature is relatively uniform in the tropics, while the subtropical area is even warmer in summer. Figure 3(b) shows the increased precipitation in the southeastern TP. There is an appearance of robust negative anomaly over Central Asia and East Asia and between them is a positive anomaly over the southern Baikal region, providing less water vapor for NC. Moreover, the anomalous anticyclonic circulation over South China indicates a strengthened WPSH tending southwards with more moisture led by lower-troposphere wind gathers in South China, as shown in Figure 4(b). This precipitation distribution agrees well with the "southern

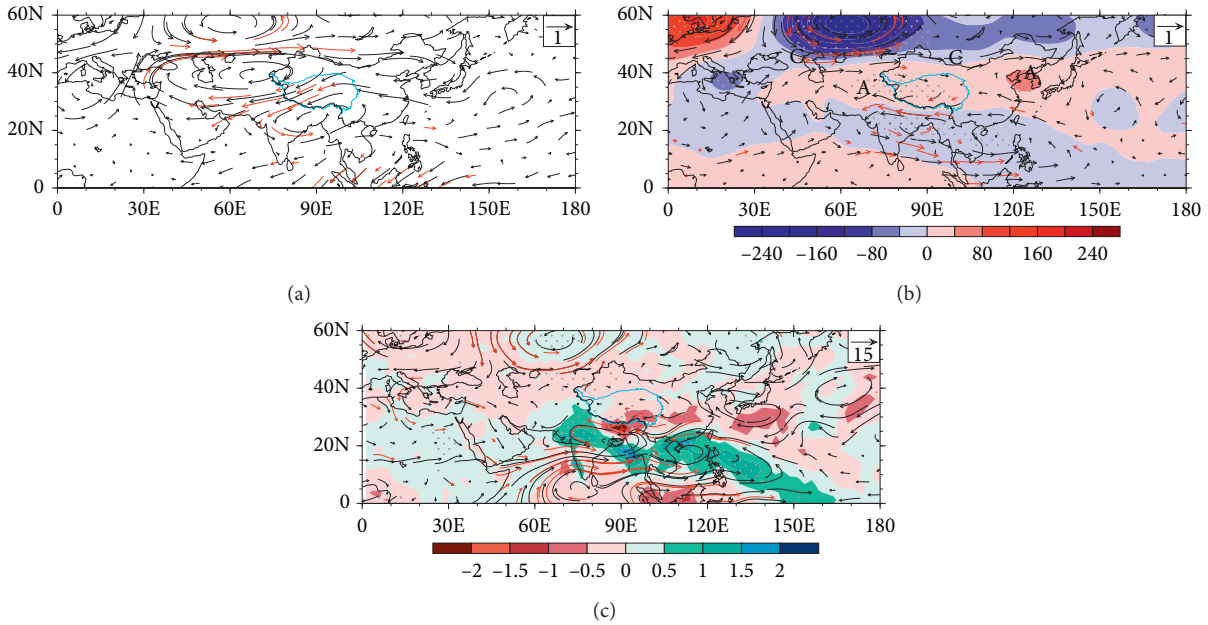

Figure 2: The linear regression pattern of the (a) 200 hPa wind (vectors, units: $m \cdot s^{-1}$), (b) The linear regression pattern of 500 hPa geopotential height (shadings, units: gpm), 500 hPa wind (vectors, units: $m \cdot s^{-1}$), and climatic JA 500 hPa geopotential height (contours, units: gpm) (c) The linear regression pattern of water flux (vectors, units: $kg \cdot m^{-1} \cdot s^{-1}$) on the PC1 during 1979–2007. Dark (light) stippling indicates values significantly exceeding the 99% (90%) confidence level using Student's t test in (b) and (c); winds with values under the 90% confidence level are omitted in (a)–(c).

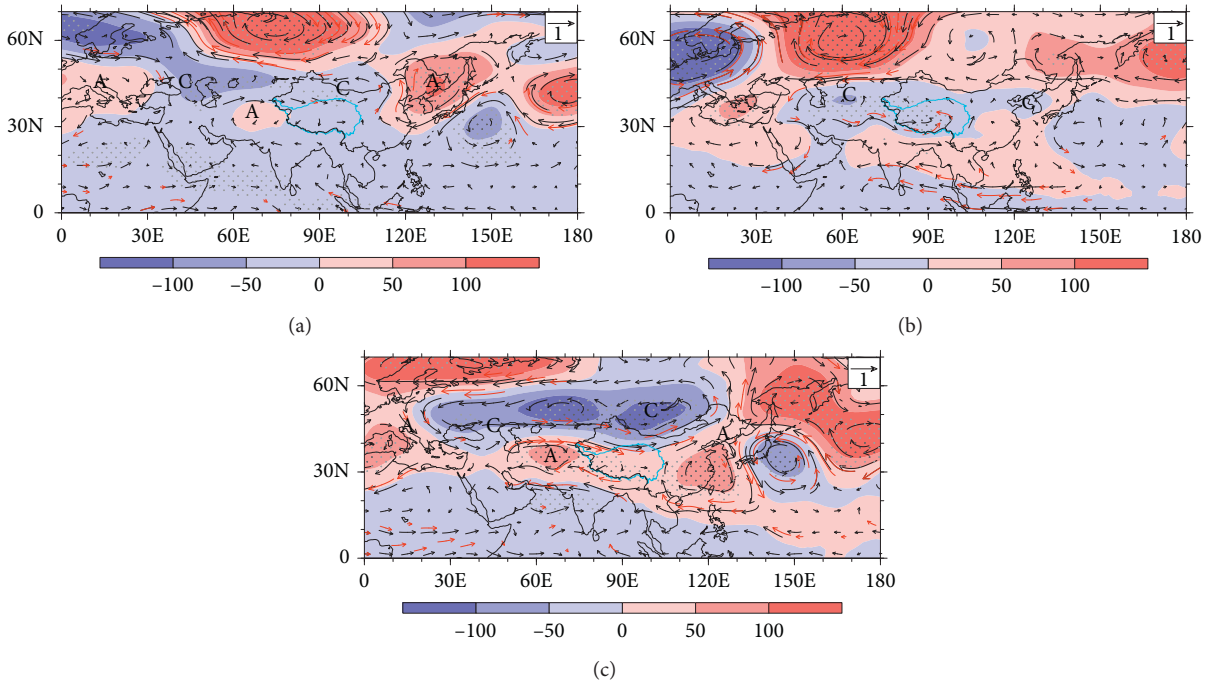

Figure 3: The linear regression pattern of the 500 hPa geopotential height (shadings, units: gpm) and 500 hPa wind (vectors, units: $m \cdot s^{-1}$) against the (a) NCR, (b) TPR, and (c) ISR for JA during 1979–2007. Dark (light) stippling indicates values significantly exceeding the 99% (90%) confidence level using Student's t test.

flood-northern drought" pattern [51, 52]. Moreover, the IS is occupied by an anomalous anticyclone, which favors the transportation of the water vapor northward (Figure 4(b)), combined with the water conveyer belt from the Bay of Bengal; it is remarkably conducive to precipitation over the southeastern TP but useless for the IS. The anomalous circulation for increased rainfall over the IS is shown in Figure 3(c). It is very similar to the result in Figure 3(a) in

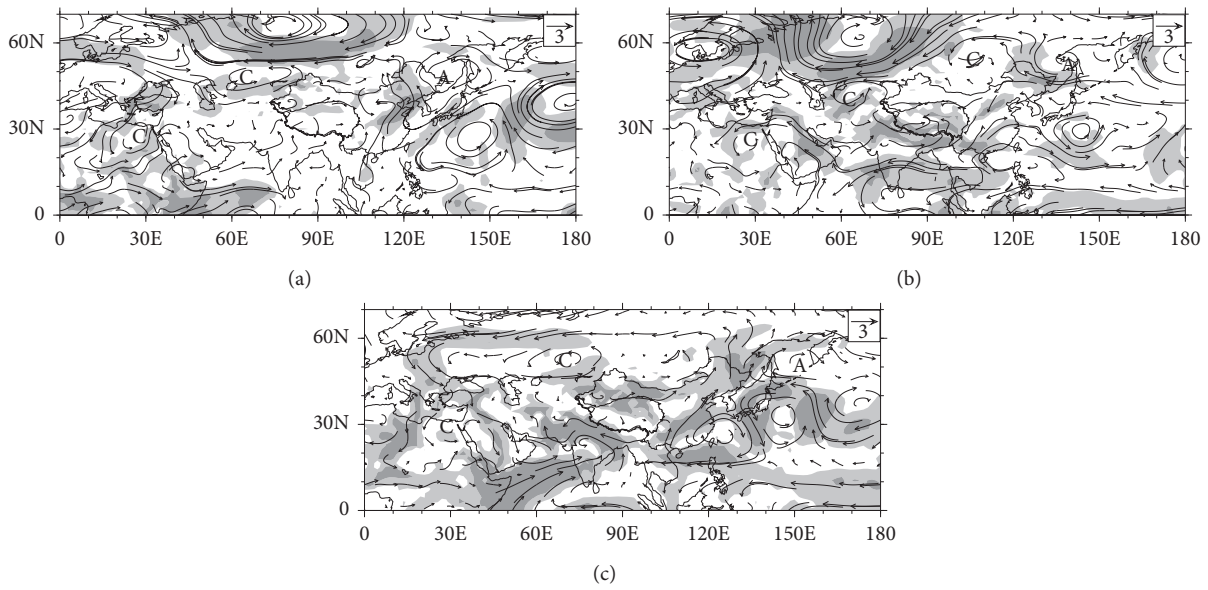

Figure 4: (a) Regression maps of 850 hPa wind (vectors, units: m·s^{-1}) anomalies against (a) NCR, (b) TPR, and (c) ISR for JA during 1979–2007. Dark (light) shadings indicate values significantly exceeding the 99% (90%) confidence level using Student's t test.

the key areas: anomalous cyclone in Baikal area, enhanced southwestern airflow in NC, anomalous anticyclone in Central Asia, cyclone anomalies in the IS, and anticyclone anomalies in northern Africa, all of which are consistent with those discussed above: on the one hand, they are conducive to precipitation in the IS; on the other hand, the divergence is conducive to the generation of Rossby wave and further affects climate in NC through wave train; only the positive anomaly is more obvious and broader in subtropical Pacific (Figure 3(c)). Meanwhile, there is a northerly air flow over the TP in the lower troposphere, as shown in Figure 4(c), implying an increase in precipitation over the IS but a decrease in precipitation over the TP. It is worth noting that there is an anomalous anticyclone over Philippines in Figures 3(a) and 3(c), just like Figure 2(b).

At middle latitude and over India, the circulation is basically the same when precipitation increases in NC and IS. That is, Central Asia, Lake Baikal, and Northeast Asia correspond to "+−+" anomaly centers, India corresponds to negative anomaly, contrary to the increase of precipitation in southeastern TP. The results further confirm the rationality of the tripole pattern, which is related to circulation at low latitudes and mid- to high-latitudes. Thus, in Section 4, we discuss the determination of the physical mechanism and highlight the tropical thermal forcing.

4. Possible Teleconnection Linking the Synergetic Diabatic Heating Effect

In the above discussion, we addressed the tripole pattern for rainfall over the IS and the southeastern TP and NC. The increased precipitation over the IS caused by strengthened ISM is often accompanied by the release of latent heating similar to that in the southeastern TP [53], which means that the diabatic heating can represent precipitation to a large extent. Therefore, we use the LBM to verify the effect of thermal forcing and investigate how it determines the rainfall distribution. Based on the tripole pattern distribution shown in Figure 1, we consider two forcings, heating over IS and cooling over TP, represent the enhancement of the ISM and the abatement of the TP heat. Q_1 and Q_2 are basic quantities for diagnosing the mechanisms of the heating process. The large centers of Q_1 and Q_2 correspond well with the heavy rainfall center of the same period of the time. The observed results of average Q_1 and Q_2 over the IS and TP are given in Figure 5 to make clear the profile of the diabatic heating in JA. It is shown that the level of the strongest heating is lower over the southeastern TP than IS. The climatic TP heating is generally near the ground, while the center is around 700 hPa over IS. We also separate the strong and weak ISM year with the 90th percentile and calculate the difference value, as shown in Figures 5(b) and 5(d), the maximum value of the TP is around 500 hPa and around 800 hPa of the IS. The average surface pressure of the climate in the southeast of the TP in summer is around 600 hPa, while that in India is around 1000 hPa. With the consideration of Q_1 and Q_2 above, we consider the changes in air heating rate caused by the two forcings are in the middle troposphere and the bottom troposphere, respectively. All these forcings have horizontal shapes that are elliptical with zonal radii of 5 degrees and meridional radii of 2 degrees. The in-depth mean and the vertical structure of the forcing are shown in Figure 6. The two forcings, respectively, represent the variations of the diabatic in the IS and southeastern TP. And, they are set to 1 K/day, just as the value in Figures 5(b) and 5(d). We performed four experiments: (1) INH, the idealized diabatic heating over India at 80°E, 22°N with the center at 0.45 (Sigma coordinate system); (2) TPC, the idealized diabatic cooling at 90°E, 30°N with the center level at 0.95; (3) TPH, same as TPC but for heating

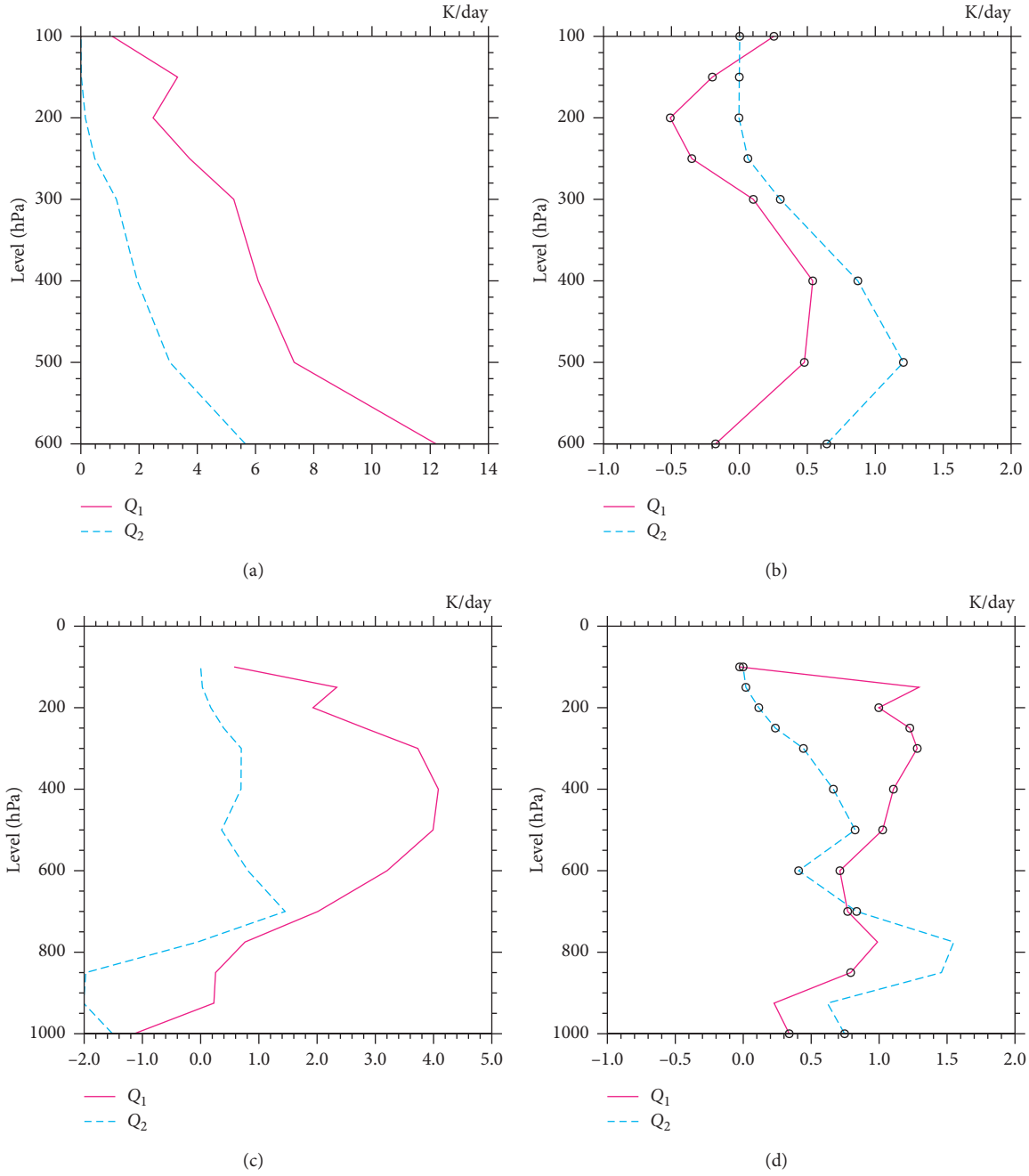

Figure 5: Profile of (a) climatological and (b) composite difference between the strong and weak ISM years of JA apparent heat source (Q_1) and apparent moisture sink (Q_2) (units: k·day^{-1}) of the atmosphere from 1979 to 2017. Black circles indicate values significantly exceeding the 90% confidence level in (b) and (d).

instead of cooling; and (4) COM, the combined forcing of INH and TPC.

We performed the INH and TPC experiments to isolate the effect of the two thermal forcings and further illustrated their synergetic effect. The results are shown in Figure 7, which are completely different for the two experiments.

For the INH experiment, there is an apparent wave train at mid- to high-latitudes, with four positive anomalies at 200 hPa (Figure 7(a)) distributed over northern Africa, Central Asia, and northern Bohai Sea, and there are three relatively weak negative anomalies in the northern Mediterranean Sea, the Baikal region, and the northwest Pacific Ocean. It is barotropic at mid- to high-latitudes in INH, and the wave train is known to be maintained by the conversion of the kinetic energy of the westerly jet stream through barotropic instability. The positive anomaly over East Asia is conducive to reinforcing the WPSH and moving northward, resulting in abundant water vapor but inadequate upward motion in NC. In the tropics, the height field of 200 hPa is symmetrical near the equator (Figure 7(a)), which may have

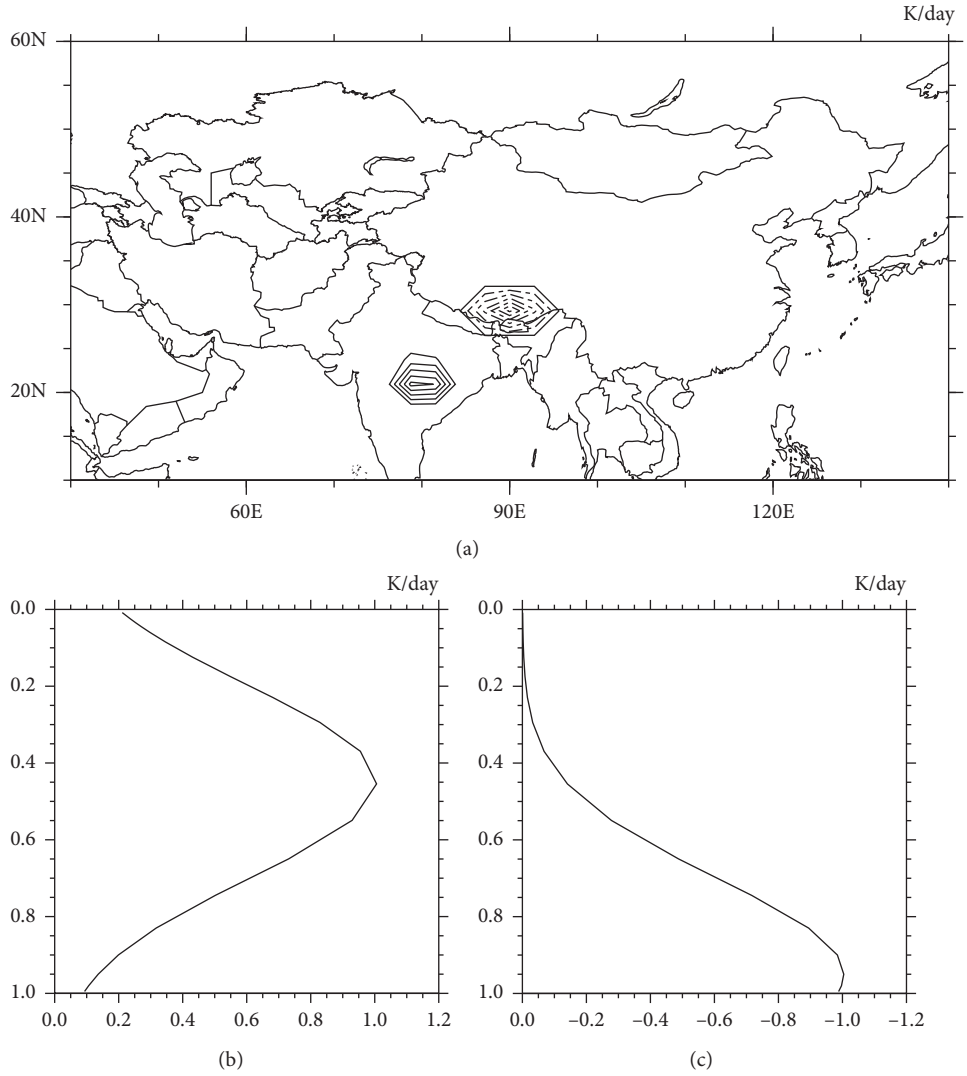

Figure 6: The (a) in-depth mean of diabatic heating anomalies in 80°E, 22°N and cooling anomalies in 90°E, 30°N (units: K·day^{-1}) and vertical profiles of forcing (units: K·day^{-1}) in (b) 80°E, 22°N and (c) 90°E, 30°N used to drive the LBM model.

triggered a Gill-type Rossby wave [54]. The Rossby wave forced by tropical thermal forcing could have been self-maintained via thermal damping, characterized by a warm temperature anomaly moving westward in the lower layer and a cold temperature anomaly moving eastward in the upper layer over West Asia (figure not shown) [55, 56]. As shown in Figure 7(b), there is a strong vertical shear of the easterly wind in North India, which increases the monsoon convection, leading to an increase in precipitation on the downshear and to the left and traps the Rossby wave in the lower troposphere. In addition, the diabatic heating associated with monsoon rainfall represented a strong forcing to the atmosphere [18, 21], leading to strengthened convection over the IS. The latent heating released by the increased rainfall, along with the land-sea thermal contrast, leads to more water vapor transport from the Southern Hemisphere and the Arabian Sea to IS as shown in Figure 7(c). And, it is coherent with the results by Greatbatch [19], in which it is interpreted that Kelvin waves appear on the Indian coast and spread eastward (Figure 7(c)). The Kelvin waves facilitate the inland transport of water vapor from the Bay of Bengal to the north and also inhibit the convection over the Philippine Sea, and the Pacific-Japan (PJ) teleconnection appears, thus strengthening the anticyclone over Japan. Additionally, it should be noted that it is baroclinic in low-latitudes except in the Sahara Desert, as shown in Figures 7(a)–7(c). The Sahara Desert in Africa has a strong heating effect and generates an easterly jet stream [57, 58] with a cyclonic shear on the south side, which can form a weather scale disturbance that propagates westward. In addition, it is important to note that there is also an external Rossby wave that propagates eastward along the westerly jet stream at mid- to high-latitudes, corresponding to the upper divergence over the North Africa.

In summer, the thermal forcing of the TP has a greater impact on the Northern Hemisphere circulation than the topography [38, 59]. The cooling at the surface may lead to weakened convection and result in less precipitation. To

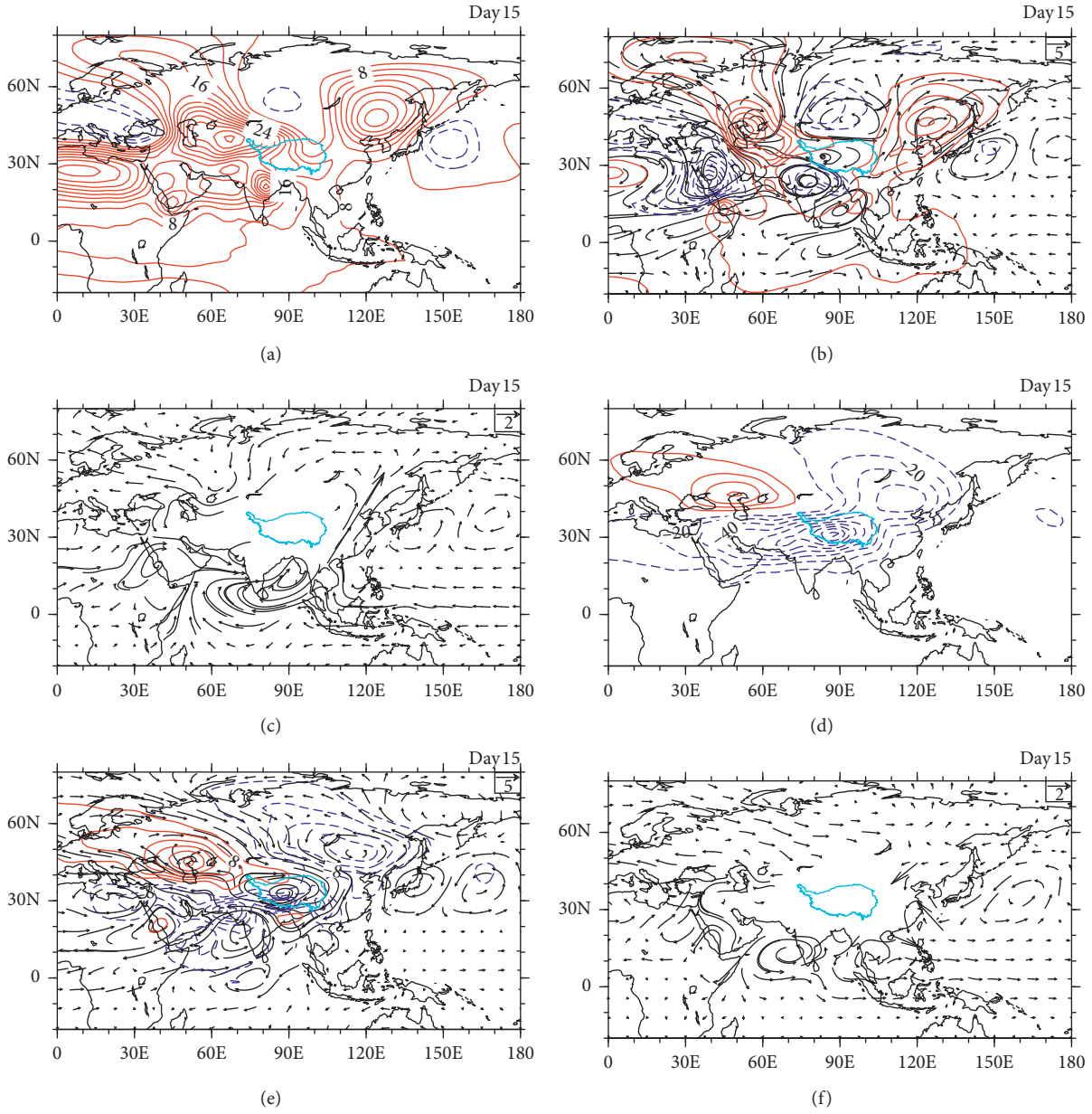

Figure 7: (a) Steady 200 hPa height anomalies (contours, unit: gpm), (b) 500 hPa height (contours, unit: gpm) and winds (vectors, unit: $m \cdot s^{-1}$) anomalies, and (c) 850 hPa winds anomalies (vectors, unit: $m \cdot s^{-1}$) generated by INH experiment, (d)–(f) is as (a)–(c), but for TPC experiment.

determine the decrease in precipitation over the southeastern TP, we performed the TPC experiment and the results are shown in the right side of Figure 7.

At the upper layer (Figure 7(d)), the negative anomaly is more obvious on a large scale and spans almost all of Asia except for the area west of Central Asia. There is a Rossby wave train at the midlatitudes moving along the westerly jet stream in the midlayer (Figure 7(e)). The anomalous cyclone in the Baikal region is stronger in the TPC. The anomalous cyclone increases the intensity of the trough but has the disadvantage of northward movement of the WPSH as shown in Figure 7(e). Moreover, an anomalous barotropic anticyclone has formed downstream from the cyclone over the Japan Sea. The water vapor is mainly concentrated in the Yangtze River basin but poor in NC. Furthermore, it generates a cyclonic anomaly in the upper troposphere over the TP, which weakens the South Asian High, suggesting a decrease in precipitation over the TP.

Therefore, both the two circulations against the two thermal forcings not only affect the local circulation but also affect the remote region. The responses to the strengthened diabatic heating over the IS are characterized by the formation of a wave train with a barotropic structure at the milatitudes, a tropical Rossby wave, easterly anomalies, Kelvin waves at low-latitudes, and PJ pattern in the Pacific. NC is at the center of positive anomalies. The significant

characteristics of TP cooling include an enhanced negative anomaly over the Baikal region, a southwestward WPSH and a weakened air-pumping effect. There are negative anomalies in East Asia. Moreover, these two forcings lead to water vapor being transported along different paths, resulting in different effects on the precipitation over NC. Thus, we designed the COM experiment to clearly determine the physical mechanism based on the tripole pattern shown in Figures 1 and 2. The time evolution diagram of the response is shown in Figure 8.

Figure 8 shows the circulation anomaly responses for the COM experiment at 500 hPa for days 1–15. On the 1st day, heating over the IS triggered an anomalous anticyclone in situ, while cooling over the southeastern TP produced an anomalous local cyclone (Figure 8(a)). On the 5th day, the original positive anomalies over India weakened substantially and moved eastward, while the negative anomaly over the TP and expanded to the southern Central Asia ranges over the TP, generating a divergence with a positive anomaly in the north (Figure 8(b)). On the 10th day, when the circulation basically formed, the divergence wind that appeared on 5th day developed an anomalous anticyclone in Central Asia, which may trigger the Rossby wave. As shown in Figure 9(a), it was symmetrical in Africa, generating a Gill-type Rossby wave. It was coherent with the suggestion by Lin et al. [20, 60] that the response over Europe was related to the equatorial Rossby wave response to ISM heating. The Gill-type Rossby wave induced the divergence over the North Africa in upper troposphere, which could induce the stationary Rossby wave. The influence of the two thermal forcings at the midlatitudes created two branches of the Rossby wave train, including the "+−+" anomalies pattern observed in West Asia, the Baikal region, and northwestern Pacific Ocean over the subtropical regions; similar patterns existed from the midlatitudes to the equator. When the response was stable on the 15th day, the Kelvin waves in India were particularly pronounced with an anomalous anticyclone over the Philippine Sea and a strengthened water vapor transport to inland (Figure 9(b)). Meanwhile, there was abundant water vapor in South Asia. It meant the water vapor in the Bay of Bengal transports to South Asia apart from converging in the IS. On the one hand, it increased precipitation in South Asia; on the other hand, it also increased water vapor of the water conveyer belt from the South China Sea to the north. The anomalous cyclone over the IS, however, caused water vapor to pass through the inland and then to the TP, leading to a deficiency in water vapor. And the positive anomalies over the TP also led the South Asian high westward, with a decreased precipitation over the TP. Furthermore, the Kelvin waves also suppressed the anticyclonic convergence over the northern Philippines and induced the PJ pattern.

Based on the simulated and the observed results displayed above, when the response was stable, the Kelvin waves led by an anomalous anticyclone over the Philippine Sea and a strengthened water vapor transport to inland (Figure 9(b)). This also has an important impact on summer precipitation in NC, and it is necessary to explore the effect of the PJ teleconnection pattern on the precipitation in NC. In this paper, the PJ pattern is defined by the EOF. The 850 hPa relative vorticity field in the East Asia-Northwest Pacific region (0–60°N, 100°E–160°E) [61–63] is calculated. Compared with the traditional definition method, the one-point correlation, regional EOF is more objective and the atmospheric variables in 850 hPa are less affected by topography and are closely related to convective precipitation; thus, it is more accurate. Then, the relative vorticity anomaly is regressed to the principal component (PC1) corresponding to the leading spatial pattern of EOF which is well separated from other modes. The obtained relative vorticity regression map presents a distinct meridional wave train in the East Asia-Pacific region, that is, PJ teleconnection pattern as shown in Figure 10(a), and it is consistent with results of Kosaka et al. [63]. The PC1 is defined as PJ teleconnection pattern index (PJI). The correlation coefficient between PJI and ISR, 0.35, is significantly a positive correlation. It is consistent with the conclusion above that the strengthening of ISM causes the Kelvin waves, and it further induces the PJ pattern. This paper mainly focuses on the pattern distribution as negative-positive-negative relative vorticity in northern Philippines, Japan Sea, and Okhotsk Sea (Figure 10(a)) corresponding to the strong ISM case. The PJ pattern has a reinforcing effect on the COM results, resulting in the negative vorticity anomaly in the south strengthened and northwestward, leading to the positive vorticity center occupying the NC. Meanwhile, the PJ pattern has a significant correlation with precipitation in China (Figure 10(b)), and the distribution of rain belt and vorticity anomalies is basically coherent. Under the joint effect of midlatitude wave train and PJ pattern (+−+ in 500 hPa, figure not shown), the positive anomaly is strengthened and moves northwestward, thus leading the WPSH moving by the same path, which is conducive to water vapor transport.

Compared with the two separate experiments discussed above (INH and TPC), the response of the COM experiment in the tropical region is almost the same as that of the INH experiment, whereas it is considerably adjusted at the midlatitudes because of TP cooling. The negative abnormal circulation is entrenched in the Baikal region, and the positive anomaly in East Asia is extended farther westward and more broadly. With the cooperation with PJ pattern, the junction of positive and negative height anomalies is just located in NC, corresponding to an anomalous cyclone at 850 hPa, suggesting a strengthened upward movement (Figure 9(b)). This result also provides support for the WPSH with northward shifting, with abundant water vapor from the western tropical Pacific Ocean to NC.

The circulation is in agreement with the regressed circulation against NCR in Figure 3(a), i.e., that type of circulation indeed leads to increased precipitation over NC. It also shows that it is indeed the synergistic effect of the two forcings to affect the summer precipitation in NC. In this subsection, the sequence of emergence of each system is explained and the rationale for the tripole pattern is described. The next step is to investigate the relationship among the anomalous circulations, how tropical forcing affects the circulation at mid- to high-latitudes and how it finally influences the precipitation over NC.

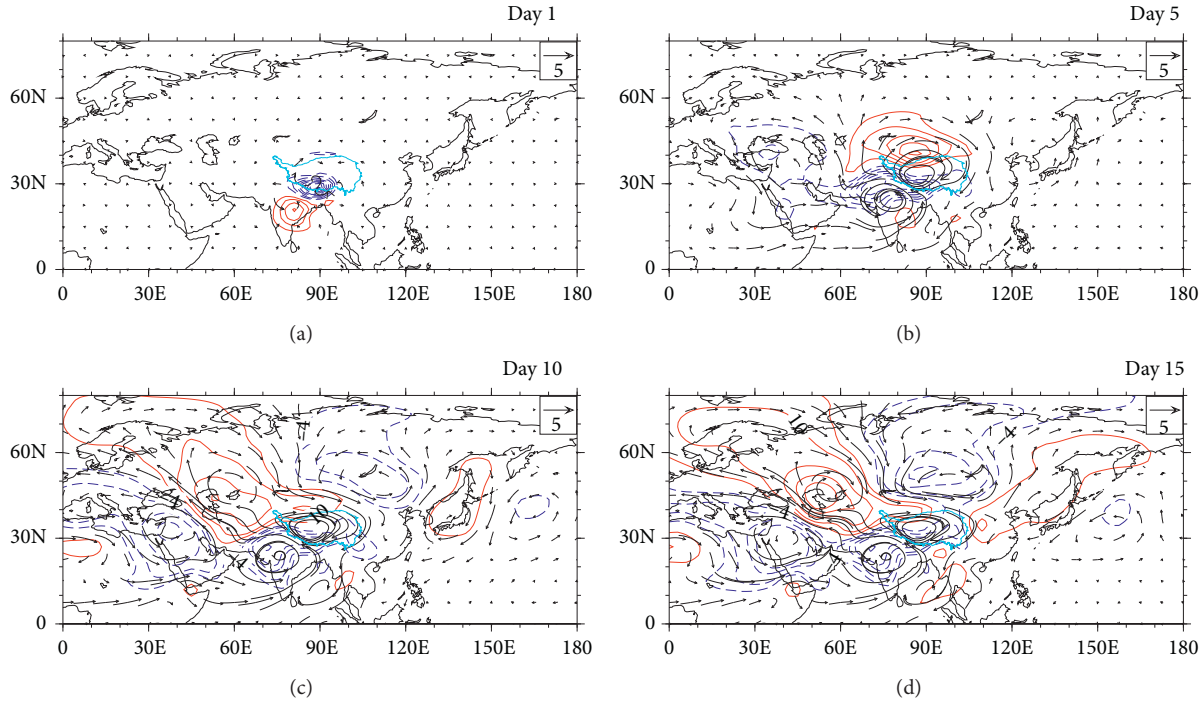

Figure 8: Steady 500 hPa height (contours, units: gpm) and 500 hPa wind (vectors, units: m·s^{-1}) anomalies generated by COM on (a) day 1, (b) day 5, (c) day 10, and (d) day 15.

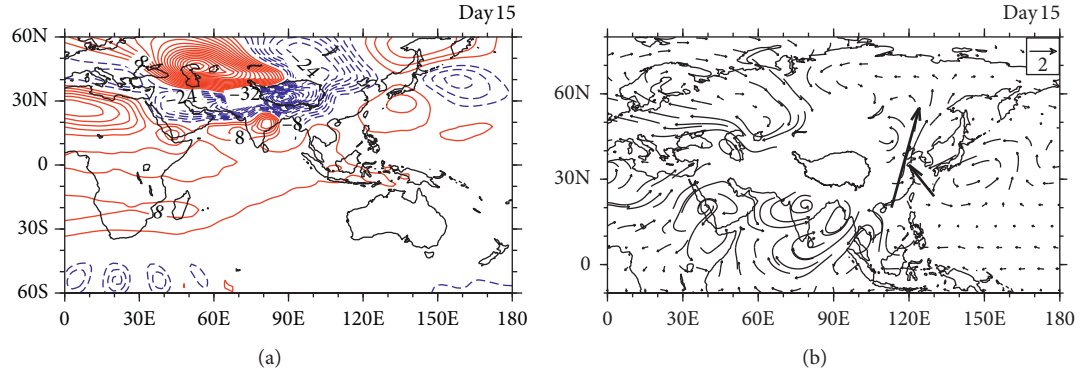

Figure 9: (a) 200 hPa height (contours, units: gpm) and (b) 850 hPa wind (vectors, units: m·s^{-1}) anomalies generated by COM experiment on day 15.

5. Investigation of the Physical Mechanisms Based on Wave Energy Propagation

Although Figure 9 provides the development of the circulation, we still do not determine the propagation of the wave train. Therefore, we calculate the Takaya and Nakamura wave activity flux (TNF) [64] and investigate the energy dispersion. The TNF regressions against precipitation indexes are shown in Figure 11. Figure 11(a) shows that for the NCR, a wave train propagates eastward originating from the Mediterranean at the midlatitudes, passes through Central Asia, and converges at the Baikal region, which is conducive to an intense cyclone there. Although the western part of the wave train is not significant at the 90% confidence level, it suggests moderate linking. Figure 11(b) is for the TPR. There is a noticeable TNF spreading southeast to Central Asia and to the TP from the high- latitude and strengthens the South Asian High. In Figure 11(c), there is an apparent eastward propagation of a Rossby wave over the midlatitudes of Eurasia. The perspective of the quasi-geostrophic stream function and TNF anomaly reveals when the ISR increases, there is a strengthened negative anomaly over the Baikal region, leading to a rising trend of rainfall over NC.

To further explore the relation between the wave activity flux and diabatic heating over the TP and the IS, the TNF results of the LBM for different forcings are calculated and are shown in Figure 12. In addition to the three forcings discussed above, we add a heat forcing over the TP as the TPH experiment but using a positive value, set as the TPC

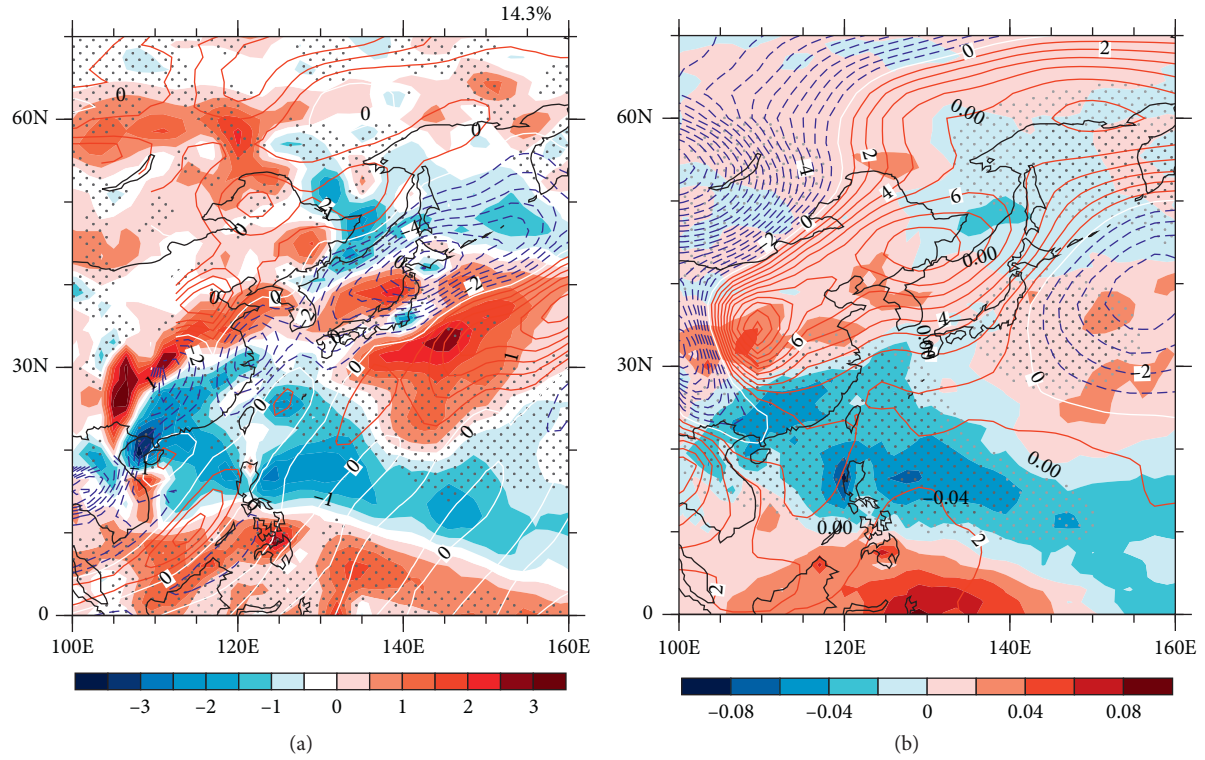

Figure 10: (a) Pacific-Japan (PJ) teleconnection patterns in JA from 1979 to 2017 (shadings) (b) JA precipitation (shadings, units: m·day^{-1}) regressed on the corresponding PJ index. Red and blue contour lines indicate positive and negative anomalies of (a) 850 hPa relative vorticity (units: 10^{-6} s^{-1}) and (b) 500 hPa height (units: gpm) generated by COM experiment on day 15. Dark (light) stippling indicates values significantly exceeding the 99% (90%) confidence level using Student's t test; the variance fraction explained by EOF1 is denoted at the top-right corner in (a).

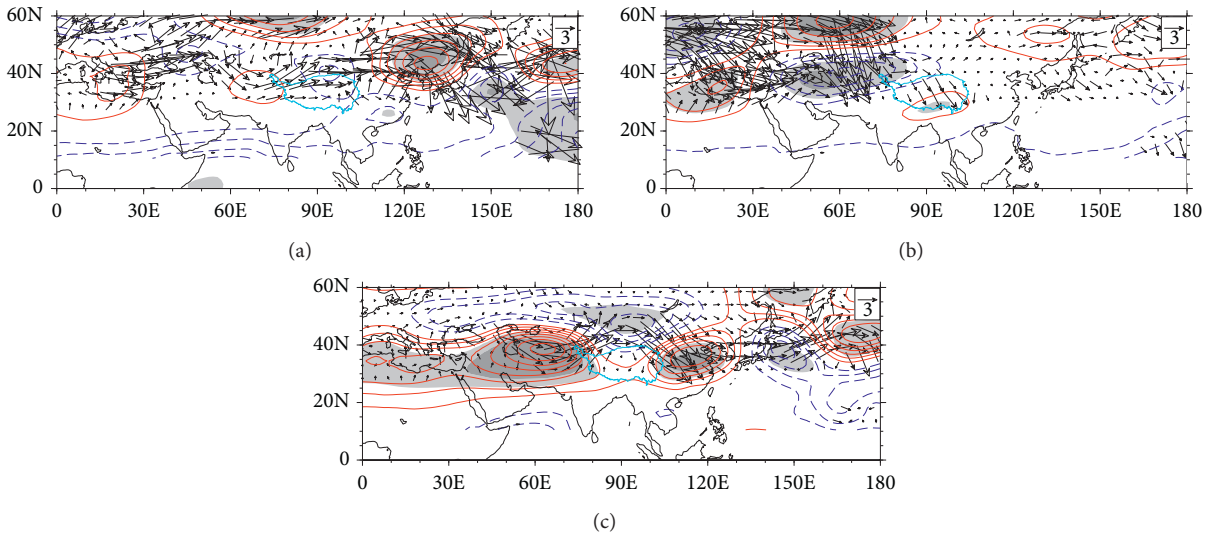

Figure 11: The linear regression pattern of the quasi-geostrophic stream function anomaly (QG) (contours, units: 10^6 m^2·s^{-1}) and T-N wave activity flux (TNF) (vectors, units: m^2·s^{-2}) at 200 hPa against (a) NCR, (b) INR, and (c) ISR. Dark (light) shadings indicate values significantly exceeding the 99% (90%) confidence level using Student's t test.

experiment. For diabatic heating over India (Figure 12(a)), the wave activity flux originates from North Africa. Then, the wave train moves to Central Asia via Europe into the subtropical jet stream, which verifies that ISM heating can trigger a midlatitude response. In the TP heating case (Figure 12(b)), there are two wave sources located in North Africa and Central Asia. The wave noticeably spreads northwestward to the west of Central Asia and then is

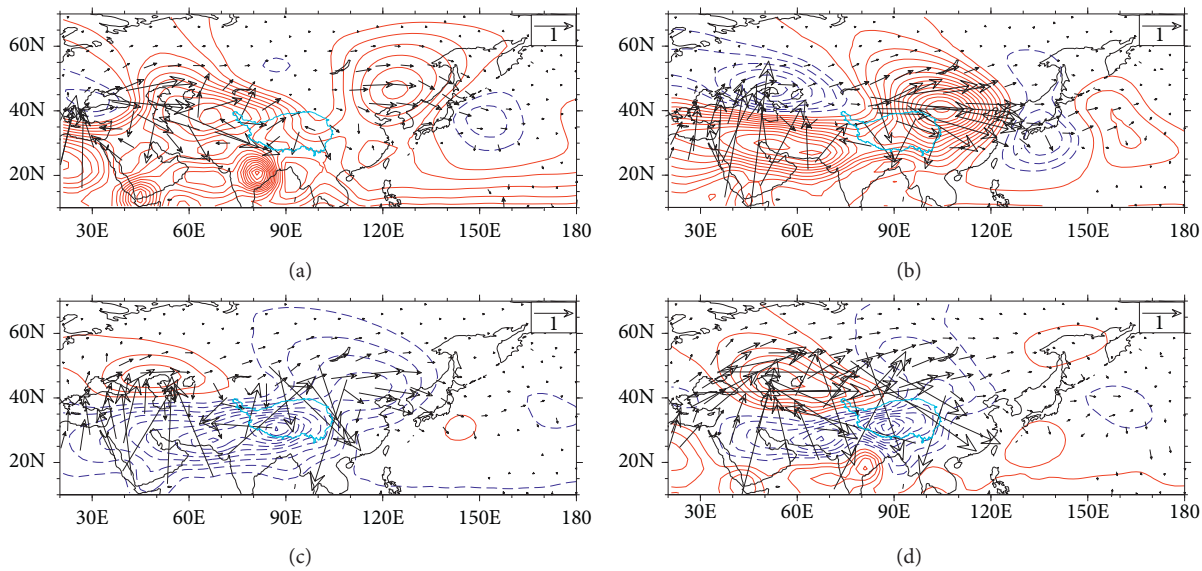

Figure 12: The QG (contours, units: $10^6\,m^2{\cdot}s^{-1}$) and TNF (vectors, units: $m^2{\cdot}s^{-2}$) at 200 hPa for (a) INH, (b) TPH, (c) TPC, and (d) COM experiments.

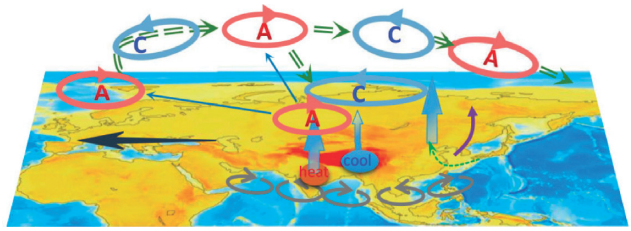

Figure 13: Schematic diagram showing the mechanism of tripole pattern. The letters denote anticyclonic and cyclonic circulation centers in 200 hPa. Black arrow denotes the easterly jet. Grey arrow denotes Kelvin waves. Purple arrow denotes PJ pattern. The green dashed arrow denotes water vapor transport.

divided into two branches. One branch spreads southeastward and enhances the South Asian High, and the other branch spreads eastward and dissipates in the Pacific Ocean, which agrees with observations well [65]. Figure 12(c) shows the results of the TPC experiment. Compared with the TPH experiment, the intensity of the TNF decreases considerably. The TPC's TNF result is similar to the result shown in Figure 11(b) but has opposite effect, which strengthens the cyclone in Baikal region. For the combined forcing (Figure 12(d)), it indicates the best agreement with observations. Heating over the IS triggers a wave train in favor of TP cooling and spreads in two directions: one is oriented southeastward to the TP and the other path is oriented along the westerly jet stream to the east, which is beneficial to the weakening of the South Asian High and the strengthening of the cyclone over the Baikal region. Thus, the propagation of the Rossby wave is the evidence for the tripole pattern.

6. Discussion and Conclusions

We obtain a clear understanding of the relationship between the ISM (i.e., precipitation over IS), TP diabatic heating (i.e., precipitation over southeastern TP), and rainfall over NC. The tripole pattern also shows some instability in some years and needs to be further explored. Moreover, the causes of the low-frequency variability of the atmosphere are diverse [66–68]. In this study, we investigate the effect of tropical heating anomalies on existing extratropical teleconnection patterns. However, the reliability of the TNF in low latitudes requires further consideration. The fact that the WPSH has been moving northward in recent years [69] also has an impact on the propagation of midlatitude wave trains. Additionally, the Rossby wave train that stretches from western Europe to West Central Asia is also caused by the strong barotropic instability at the jet stream exit region in the North Atlantic Ocean [30]. Therefore, further studies are required to determine the relationships among the different resources.

Based on 56 years of JA precipitation, this study explains the IS-TP-NC tripole pattern. The ISM and the TP are both important heating sources in Asia and are interactive. Thus, they are considered as one system and the synergy effect of the ISM and TP heating is the focus of this study. In this study, we analyze the mechanism of the formation of this tripole pattern from the perspectives of circulation, LBM numerical experiments, and wave propagation. According to the results, the formation of the tripole pattern is caused by a synergy effect of diabatic heating over the IS and the TP.

The sketch map shown in Figure 13 illustrates the mechanism of the tripolar pattern. In summer, increased precipitation over the IS is corresponding to decreased precipitation over the southeastern TP, i.e., an enhanced ISM and a decrease in southeastern TP thermal forcing and vice versa. In the first case, there is enhanced convection and easterlies over the IS. The baroclinic structure at low-latitudes produces strong upward movement as a result of the strengthened vertical wind shear. Moreover, a Gill-type Rossby wave is generated and propagates westward along the

abnormal easterlies to North Africa. This leads to a divergence in the higher troposphere, which triggers an external Rossby wave and moves eastward and is maintained by extracting the kinetic energy of the basic zonal flow. In addition, the strengthened ISM is benefit to the divergence over Central Asia, and this would further reinforce the wave train. The wave train affects the distribution of the circulation at the midlatitudes with the PJ pattern induced by strengthened ISM. Thus, there is a cyclonic anomaly over the Baikal region and an anticyclonic anomaly over the North Pacific Ocean, leading to abundant water vapor transport and sufficient upward movement over NC. Additionally, one of the wave trains is oriented southeastward to the TP, weakening the South Asian High.

Data Availability

The data used to support the findings of this study are available from the corresponding author upon request.

Conflicts of Interest

The authors declare that they have no conflicts of interest.

Acknowledgments

This research was jointly supported by the National Key R&D Program of China (Grant no. 2016YFA0600702), the National Natural Science Foundation of China for Key Program (Grant nos. 41630426 and 41975083), and the Qing Lan Project and the Priority Academic Program Development of the Jiangsu Higher Education Institutions (PAPD).

References

[1] Y. Wang, "Effects of blocking anticyclones in Eurasia in the rainy season (Meiyu/Baiu season)," *Journal of the Meteorological Society of Japan. Ser. II*, vol. 70, no. 5, pp. 929–951, 1992.

[2] N. Sato and M. Takahashi, "Dynamical processes related to the appearance of quasi-stationary waves on the subtropical jet in the midsummer northern hemisphere," *Journal of Climate*, vol. 19, no. 8, pp. 1531–1544, 2006.

[3] L. Pei, Z. W. Yan, and H. Yang, "Multidecadal variability of dry/wet patterns in eastern China and their relationship with the Pacific decadal oscillation in the last 413 years (in Chinese)," *Chinese Science Bulletin*, vol. 60, pp. 97–108, 2015, in Chinese.

[4] Y. Ding, "Summer monsoon rainfalls in China," *Journal of the Meteorological Society of Japan. Ser. II*, vol. 70, no. 1B, pp. 373–396, 1992.

[5] R. H. Kripalani and A. Kulkarni, "Monsoon rainfall variations and teleconnections over south and east Asia," *International Journal of Climatology*, vol. 21, no. 5, pp. 603–616, 2001.

[6] R. H. Zhang, "Relations of water vapor transport from Indian monsoon with that over east Asia and summer rainfall in China," *Advances in Atmospheric Sciences*, vol. 18, no. 5, pp. 1005–1007, 2001.

[7] W. Zhou, W. Chen, and D. X. Wang, "The implications of El Niño-southern oscillation signal for south China monsoon climate," *Aquatic Ecosystem Health & Management*, vol. 15, no. 1, pp. 14–19, 2012.

[8] J. Zhang, C. Liu, and H. Chen, "The modulation of Tibetan plateau heating on the multi-scale northernmost margin activity of East Asia summer monsoon in northern China," *Global and Planetary Change*, vol. 161, pp. 149–161, 2018.

[9] Q. Ding and B. Wang, "Circumglobal teleconnection in the northern hemisphere summer," *Journal of Climate*, vol. 18, no. 17, pp. 3483–3505, 2005.

[10] G. Chen and R. Huang, "Excitation mechanisms of the teleconnection patterns affecting the july precipitation in northwest China," *Journal of Climate*, vol. 25, no. 22, pp. 7834–7851, 2012.

[11] I. M. Held, "Stationary and quasi-stationary eddies in the extratropical troposphere theory," in *Large-Scale Dynamical Processes in the Atmosphere*, B. J. Hoskins and R. P. Pearce, Eds., pp. 127–168, Academic Press, London, UK, 1983.

[12] B. J. Hoskins and T. Ambrizzi, "Rossby wave propagation on a realistic longitudinally varying flow," *Journal of the Atmospheric Sciences*, vol. 50, no. 12, pp. 1661–1671, 1993.

[13] T. Enomoto, "Interannual variability of the Bonin high associated with the propagation of Rossby waves along the Asian jet," *Journal of the Meteorological Society of Japan*, vol. 82, no. 4, pp. 1019–1034, 2004.

[14] Q. Ding, B. Wang, J. M. Wallace, and G. Branstator, "Tropical-extratropical teleconnections in boreal summer: observed interannual variability," *Journal of Climate*, vol. 24, no. 7, pp. 1878–1896, 2011.

[15] R. H. Kripalani and S. V. Singh, "Large scale aspects of India-China summer monsoon rainfall," *Advances in Atmospheric Sciences*, vol. 10, no. 1, pp. 71–84, 1993.

[16] B. Wang, R. Wu, and K.-M. Lau, "Interannual variability of the Asian summer monsoon: contrasts between the Indian and the western North Pacific-East Asian monsoons," *Journal of Climate*, vol. 14, no. 20, pp. 4073–4090, 2001.

[17] Y. Y. Liu and Y. H. Ding, "Analysis and numerical simulation of the teleconnection between Indian summer monsoon and precipitation in North China," *Acta Meteorological Sinica*, vol. 66, no. 5, pp. 789–799, 2008, in Chinese.

[18] R. H. Kripalani, A. Kulkarni, and S. V. Singh, "Association of the Indian summer monsoon with the northern hemisphere mid-latitude circulation," *International Journal of Climatology*, vol. 17, no. 10, pp. 1055–1067, 1997.

[19] R. J. Greatbatch, X. Sun, and X.-Q. Yang, "Impact of variability in the Indian summer monsoon on the East Asian summer monsoon," *Atmospheric Science Letters*, vol. 14, no. 1, pp. 14–19, 2013.

[20] H. Lin and Z. Wu, "Indian summer monsoon influence on the climate in the North Atlantic-European region," *Climate Dynamics*, vol. 39, no. 1-2, pp. 303–311, 2012.

[21] T. T. Han, S. He, H. Wang, and X. Hao, "Enhanced influence of early-spring tropical Indian ocean SST on the following early-summer precipitation over Northeast China," *Climate Dynamics*, vol. 51, no. 11, pp. 4065–4076, 2018.

[22] K.-S. Yun, S.-Y. Kim, K.-J. Ha, and M. Watanabe, "Effects of subseasonal basic state changes on Rossby wave propagation during northern summer," *Journal of Geophysical Research: Atmospheres*, vol. 116, no. D24, 2011.

[23] J. Yang, Q. Liu, Z. Liu, L. Wu, and F. Huang, "Basin mode of Indian ocean sea surface temperature and northern hemisphere circumglobal teleconnection," *Geophysical Research Letters*, vol. 36, no. 19, 2009.

[24] G. Chen, R. Huang, and L. Zhou, "Baroclinic instability of the silk road pattern induced by thermal damping," *Journal of the Atmospheric Sciences*, vol. 70, no. 9, pp. 2875–2893, 2013.

[25] R. Wu, "A mid-latitude Asian circulation anomaly pattern in boreal summer and its connection with the Indian and East Asian summer monsoons," *International Journal of Climatology*, vol. 22, no. 15, pp. 1879–1895, 2002.

[26] M. Yanai and C. Li, "Mechanism of heating and the boundary layer over the Tibetan plateau," *Monthly Weather Review*, vol. 122, no. 2, pp. 305–323, 1994.

[27] G. Wu, Y. Liu, B. He, Q. Bao, A. Duan, and F.-F. Jin, "Thermal controls on the Asian summer monsoon," *Scientific Reports*, vol. 2, no. 1, 2012.

[28] M. Lu, S. Yang, Z. Li, B. He, S. He, and Z. Wang, "Possible effect of the Tibetan plateau on the "upstream" climate over West Asia, North Africa, south Europe and the north Atlantic," *Climate Dynamics*, vol. 51, no. 4, pp. 1485–1498, 2017.

[29] J. Zhang, Q. Tang, H. Chen, and S. Liu, "Northward shift in circulation system over the Asian mid-latitudes linked to an increasing heating anomaly over the northern Tibetan plateau during the past two decades," *International Journal of Climatology*, vol. 37, no. 2, pp. 834–848, 2016.

[30] J. Zhang, Y. Jiang, H. Chen, and Z. Wu, "Double-mode adjustment of Tibetan plateau heating to the summer circumglobal teleconnection in the northern hemisphere," *International Journal of Climatology*, vol. 38, no. 2, pp. 663–676, 2018.

[31] P. Chen, "Thermally forced stationary waves in a quasigeostrophic system," *Journal of the Atmospheric Sciences*, vol. 58, no. 12, pp. 1585–1594, 2001.

[32] G. Wu, Y. Liu, Q. Zhang et al., "The influence of mechanical and thermal forcing by the Tibetan plateau on Asian climate," *Journal of Hydrometeorology*, vol. 8, no. 4, pp. 770–789, 2007.

[33] X. Zhu, O. Bothe, and K. Fraedrich, "Summer atmospheric bridging between Europe and east Asia: influences on drought and wetness on the Tibetan plateau," *Quaternary International*, vol. 236, no. 1-2, pp. 151–157, 2011.

[34] Z. S. An, J. E. Kutzbach, W. L. Prell, and S. C. Porter, "Evolution of Asian monsoons and phased uplift of the Himalaya–Tibetan plateau since late Miocene times," *Nature*, vol. 411, no. 6833, pp. 62–66, 2001.

[35] B. Wang, Q. Bao, B. Hoskins, G. Wu, and Y. Liu, "Tibetan plateau warming and precipitation changes in East Asia," *Geophysical Research Letters*, vol. 35, no. 14, 2008.

[36] T. Yao, V. Masson-Delmotte, J. Gao et al., "A review of climatic controls on δ18O in precipitation over the Tibetan plateau: observations and simulations," *Reviews of Geophysics*, vol. 51, no. 4, pp. 525–548, 2013.

[37] X. Jiang and M. Ting, "A dipole pattern of summertime rainfall across the Indian subcontinent and the Tibetan plateau," *Journal of Climate*, vol. 30, no. 23, pp. 9607–9620, 2017.

[38] L. Zhou, H. Zou, S. Ma et al., "The observed impacts of South Asian summer monsoon on the local atmosphere and the near-surface turbulent heat exchange over the Southeast Tibet," *Journal of Geophysical Research*, vol. 120, no. 22, pp. 11509–11518, 2015.

[39] L. Feng and T. Zhou, "Water vapor transport for summer precipitation over the Tibetan plateau: multidata set analysis," *Journal of Geophysical Research: Atmospheres*, vol. 117, no. D20, 2012.

[40] W. Dong, Y. Lin, J. S. Wright et al., "Summer rainfall over the southwestern Tibetan plateau controlled by deep convection over the Indian subcontinent," *Nature Communications*, vol. 7, no. 1, p. 10925, 2016.

[41] A. Yatagai, K. Kamiguchi, O. Arakawa, A. Hamada, N. Yasutomi, and A. Kitoh, "APHRODITE: constructing a long-term daily gridded precipitation dataset for Asia based on a dense network of rain gauges," *Bulletin of the American Meteorological Society*, vol. 93, no. 9, pp. 1401–1415, 2012.

[42] A. Becker, P. Finger, A. Meyerchristoffer et al., "A description of the global land–surface precipitation data products of the global precipitation climatology center with sample applications including centennial (trend) analysis from 1901–present," *Earth System Sciences Data Discussions*, vol. 5, no. 2, pp. 921–998, 2013.

[43] R. Adler, M. Sapiano, G. Huffman et al., "The global precipitation climatology project (GPCP) monthly analysis (new version 2.3) and a review of 2017 global precipitation," *Atmosphere*, vol. 9, no. 4, p. 138, 2018.

[44] D. P. Dee, Uppala, S. Simmons et al., "The ERA–interim reanalysis: configuration and performance of the data assimilation system," *Quarterly Journal of the Royal Meteorological Society*, vol. 137, pp. 553–559, 2011.

[45] G. R. North, T. L. Bell, R. F. Cahalan, and F. J. Moeng, "Sampling errors in the estimation of empirical orthogonal functions," *Monthly Weather Review*, vol. 110, no. 7, pp. 699–706, 1982.

[46] M. Yanai, S. Esbensen, and J.-H. Chu, "Determination of bulk properties of tropical cloud clusters from large-scale heat and moisture budgets," *Journal of the Atmospheric Sciences*, vol. 30, no. 4, pp. 611–627, 1973.

[47] M. Watanabe and M. Kimoto, "Atmosphere-ocean thermal coupling in the North Atlantic: a positive feedback," *Quarterly Journal of the Royal Meteorological Society*, vol. 126, no. 570, pp. 3343–3369, 2000.

[48] M. Watanabe and M. Kimoto, "Corrigendum," *Quarterly Journal of the Royal Meteorological Society*, vol. 127, pp. 733-734, 2001.

[49] M. Watanabe and F.-F. Jin, "A moist linear baroclinic model: coupled dynamical-convective response to El Niño," *Journal of Climate*, vol. 16, no. 8, pp. 1121–1139, 2003.

[50] J. Zhang, H. Chen, and S. Zhao, "A tripole pattern of summertime rainfall and the teleconnections linking northern China to the Indian subcontinent," *Journal of Climate*, vol. 32, no. 12, pp. 3637–3653, 2019.

[51] H. J. Wang, "The instability of the East Asian summer monsoon–ENSO relations," *Advances in Atmospheric Sciences*, vol. 19, no. 1, pp. 1–11, 2002.

[52] Y. Ding, Y. Sun, Z. Wang, Y. Zhu, and Y. Song, "Inter-decadal variation of the summer precipitation in China and its association with decreasing Asian summer monsoon part II: possible causes," *International Journal of Climatology*, vol. 29, no. 13, pp. 1926–1944, 2009.

[53] Y. Liu, G. Wu, J. Hong et al., "Revisiting Asian monsoon formation and change associated with Tibetan plateau forcing: II. Change," *Climate Dynamics*, vol. 39, no. 5, pp. 1183–1195, 2012.

[54] A. E. Gill, "Some simple solutions for heat-induced tropical circulation," *Quarterly Journal of the Royal Meteorological Society*, vol. 106, no. 449, pp. 447–462, 1980.

[55] I. M. Held, R. T. Pierrehumbert, and R. L. Panetta, "Dissipative destabilization of external Rossby waves," *Journal of the Atmospheric Sciences*, vol. 43, no. 4, pp. 388–396, 1986.

[56] W. A. Robinson, "Two applications of potential vorticity thinking," *Journal of the Atmospheric Sciences*, vol. 44, no. 11, pp. 1554–1557, 1987.

[57] K. H. Cook, "Generation of the African easterly jet and its role in determining west African precipitation," *Journal of Climate*, vol. 12, no. 5, pp. 1165–1184, 1999.

[58] C. Thorncroft and M. Blackburn, "Maintenansce of the African easterly jet," *Quarterly Journal of the Royal Meteorological Society*, vol. 125, no. 555, pp. 763–786, 1999.

[59] G. X. Wu, W. Li, H. Guo, H. Liu, J. Xue, and Z. Wang, "Sensible heat driven air–pump over the Tibetan plateau and its impacts on the Asian summer monsoon (in Chinese)," in *Collection in Memory of Zhao Jiuzhang*, Y. Duzheng, Ed., pp. 116–126, Chinese Science Press, Beijing, China, 1997.

[60] H. Lin, "Global extratropical response to diabatic heating variability of the Asian summer monsoon," *Journal of the Atmospheric Sciences*, vol. 66, no. 9, pp. 2697–2713, 2009.

[61] Y. Kosaka and H. Nakamura, "Structure and dynamics of the summertime Pacific-Japan teleconnection pattern," *Quarterly Journal of the Royal Meteorological Society*, vol. 132, no. 619, pp. 2009–2030, 2006.

[62] Y. Kosaka and H. Nakamura, "Mechanisms of meridional teleconnection observed between a summer monsoon system and a subtropical anticyclone. Part I: the pacific-Japan pattern," *Journal of Climate*, vol. 23, no. 19, pp. 5085–5108, 2010.

[63] Y. Kosaka, S.-P. Xie, N.-C. Lau, and G. A. Vecchi, "Origin of seasonal predictability for summer climate over the northwestern Pacific," *Proceedings of the National Academy of Sciences*, vol. 110, no. 19, pp. 7574–7579, 2013.

[64] K. Takaya and H. Nakamura, "A formulation of a phase-independent wave-activity flux for stationary and migratory quasigeostrophic eddies on a zonally varying basic flow," *Journal of the Atmospheric Sciences*, vol. 58, no. 6, pp. 608–627, 2001.

[65] Q. Ding and B. Wang, "Intraseasonal teleconnection between the summer Eurasian wave train and the Indian monsoon," *Journal of Climate*, vol. 20, no. 15, pp. 3751–3767, 2007.

[66] I. M. Held, S. W. Lyons, and S. Nigam, "Transients and the extratropical response to El Niño," *Journal of the Atmospheric Sciences*, vol. 46, no. 1, pp. 163–174, 1989.

[67] K. L. Swanson, "Stationary wave accumulation and the generation of low-frequency variability on zonally varying flows," *Journal of the Atmospheric Sciences*, vol. 57, no. 14, pp. 2262–2280, 2000.

[68] K. L. Swanson, "Oscillatory instabilities to zonally varying barotropic flows," *Journal of the Atmospheric Sciences*, vol. 58, no. 21, pp. 3135–3147, 2001.

[69] B. Zhou, Y. Xu, and Y. Shi, "Present and future connection of Asian-Pacific oscillation to large-scale atmospheric circulations and East Asian rainfall: results of CMIP5," *Climate Dynamics*, vol. 50, no. 1-2, pp. 17–29, 2017.